JOURNAL OF SYNCHROTRON RADIATION
ISSN 1600-5775

Demonstration of high-performance pole pieces made of monocrystalline dysprosium for short-period undulators

Takashi Tanaka[a]* and Akihiro Kagamihata[b]

[a]RIKEN SPring-8 Center, Koto 1-1-1, Sayo, Hyogo 679-5148, Japan, and [b]Japan Synchrotron Radiation Research Institute, Koto 1-1-1, Sayo, Hyogo 679-5198, Japan. *Correspondence e-mail: ztanaka@spring8.or.jp

Received 10 October 2018
Accepted 30 April 2019

Edited by S. Svensson, Uppsala University, Sweden

Keywords: short-period undulators; high-performance pole pieces; monocrystalline dysprosium.

Reported here are the results of experiments carried out to demonstrate the magnetic performance of dysprosium (Dy) to enhance the capability of undulators. Tiny pieces of monocrystalline Dy surrounded by permanent magnets (PMs) work as pole pieces (PPs) to concentrate the magnetic flux, when cooled down below the Curie temperature of 85 K. A PP made of Dy is much more attractive than one made of a conventional material, because its saturation magnetization is much higher. Furthermore, it also allows for a more flexible selection of PM material, potentially leading to further enhancement of the performance of short-period undulators. Besides these advantages, practical issues related to using Dy PPs and countermeasures against them are discussed.

1. Introduction

Dysprosium (Dy) is a rare earth element having the highest magnetic moment among the possible magnetic materials generally available. For example, the saturated magnetic flux density (B_s) of Dy exceeds 3.5 T below the Curie temperature of 85 K (Behrendt *et al.*, 1958); this is about 50% larger than the value of B_s = 2.35 T for vanadium Peremdur (VP), which is widely used as a high-B_s material. It is obvious that replacing VP with Dy will enhance the performance of magnetic devices, and thus such applications of Dy have been explored for a long time.

One of the possible applications is the so-called undulator, which generates a sinusoidal magnetic field and deflects a high-energy electron beam to produce intense synchrotron radiation. Nowadays, pole pieces (PPs) made of VP are often used in undulators to concentrate the magnetic flux generated by permanent magnets (PMs) and enhance the peak magnetic field. If Dy could be used as the PP material, the attainable peak field could be further enhanced. It should be noted, however, that Dy has a strong magnetic anisotropy with the $\langle 11\bar{2}0 \rangle$ orientation corresponding to the easy axis of magnetization. As a result, we need monocrystalline Dy (MXDy), or at least highly crystalline Dy, so that PPs made of Dy are practically effective in undulators.

It is easy to understand that simply replacing VP with MXDy is not cost effective, which is the reason why a number of studies have been made (O'Shea *et al.*, 2013; Murokh *et al.*, 2014) to utilize 'textured' Dy generated by annealing a polycrystalline Dy foil (Swift & Mathur, 1974). The experimental results of these studies have shown that, although textured Dy has a better magnetic performance than VP, the achieved performance is just a few percent better than that with conventional VP PPs for an undulator sample with a period of

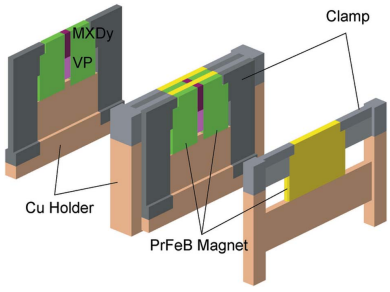

© 2019 International Union of Crystallography

8 mm; this is because the initial permeability μ_i of textured Dy is not sufficiently high, which is also reported for commercially available rolled Dy foils (Bahrdt, 2011).

The above results suggest that a much better performance is expected with PPs made of MXDy instead of textured Dy, although we need to explore a realistic and cost-effective way of fabricating them. In this paper, we discuss the design of PM undulators to take advantage of the excellent magnetic properties of MXDy as an undulator PP, and present the results of experiments carried out to demonstrate their performance. We also discuss practical issues related to MXDy PPs, together with possible countermeasures against them.

2. Undulator magnetic design for MXDy PPs

Let us first discuss the conventional undulator design using VP PPs, as shown in Fig. 1(*a*), where λ_u is the magnetic period, and the rectangles with and without arrows denote PMs and PPs, respectively. The coordinate system to be used in the following discussion is also shown: z denotes the longitudinal direction along which the electron beam is injected, while x and y denote the horizontal and vertical directions perpendicular to z. The lengths of the PMs and PPs, L_m and L_p, respectively, are optimized to maximize the peak magnetic field, and are roughly given by $L_m = (1/4–1/3)\lambda_u$ and $L_p = (1/6–1/4)\lambda_u$. The heights H_m and H_p are chosen to be long enough so that the resultant peak magnetic field is similar to what is obtained with an infinitely large height, and are in general of the order of λ_u. The widths W_m and W_p should be wide enough to obtain a sufficiently good field uniformity, and are typically of the order of 30 mm or larger.

Based on the conventional design described above, the cross-sectional area of the PP (H_pW_p) should be at least larger than 300 mm^2, assuming λ_u = 10 mm as an example. Recalling that the maximum dimensions of a single piece of MXDy grown by a common method are at most 10 mm in each direction, it is obvious that replacing VP PPs with MXDy ones is unrealistic in the conventional design.

Now let us consider the magnetic design illustrated in Fig. 1(*b*), where the width of the PP is shortened and additional side magnets are inserted; note that the additional magnets are drawn partially transparent in the side view to visualize the inside. In this design, each PP is divided into two parts, *i.e.* inner and outer PPs, the former of which has a height of H_d and is shown in the hatched area. The cross-sectional area of the inner PP (H_dW_p) can be reduced down to 10 mm^2 or less, and thus it can be replaced with a single piece of MXDy to enhance the peak magnetic field. In practice, we have to make a compromise in specifying the height of the MXDy (H_d) between the attainable performance and the required volume of the MXDy.

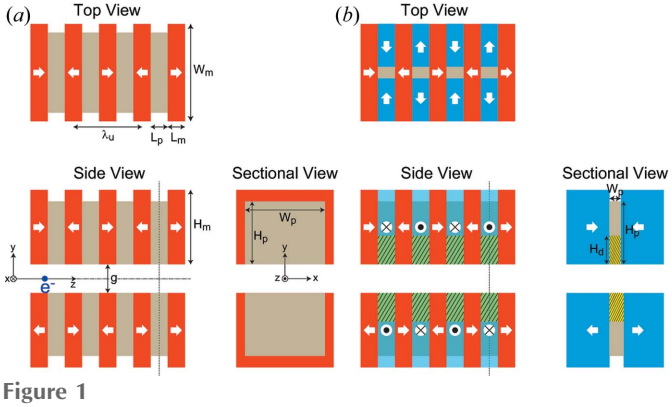

Figure 1
The magnetic circuit of (*a*) a conventional undulator with PPs made of VP, and (*b*) the new undulator with narrower PPs made of MXDy (inner) and VP (outer).

It should be mentioned here that field enhancement by a narrow PP combined with side magnets is not particularly new; high-field wigglers equipped with side magnets, even though with a relatively long period, have been built before (Nakamura *et al.*, 1998; Chang *et al.*, 1998; Chavanne *et al.*, 1999). Applications to a much shorter period have also been explored based on numerical studies (Hara *et al.*, 2004; Murokh *et al.*, 2014), including the utilization of bimaterial PPs (Bahrdt, 2011), although they have not been experimentally demonstrated.

To activate the MXDy PPs in this undulator design, the whole structure should be cooled down below the Curie temperature of Dy; this is readily compatible with the so-called cryogenic permanent magnet undulators (CPMUs), in which PMs are placed inside the vacuum chamber and cooled down for the purpose of enhancing the remanence (B_r) and coercivity (H_{cj}). Since the first proposal in 2004 (Hara *et al.*, 2004), a number of CPMUs have been built using neodymium–iron–boron (NdFeB) PMs (Chavanne *et al.*, 2009; Ostenfeld & Pedersen, 2010; Calvi *et al.*, 2013) and praseodymium–iron–boron (PrFeB) PMs (Bahrdt & Kuhn, 2015; Benabderrahmane *et al.*, 2017). Note that the B_r of NdFeB PMs drops below ∼135 K, owing to the spin reorientation effect (García *et al.*, 2000). This is the reason why PrFeB PMs, which do not show spin reorientation, attract more attention for application to CPMUs. Obviously, PrFeB PMs should be chosen in the proposed scheme as well.

We now discuss another advantage of MXDy against VP as the PP material, which is particularly important for short-period undulators. It is well known that PMs in undulators are exposed to a strong reverse field generated by adjacent PMs, as seen in Fig. 1. What is more critical in the conventional design is that the reverse field acting on the inner surface facing the electron beam is locally enhanced by the PPs inserted between PMs. This is illustrated in Fig. 2(*a*), showing the bottom half of the magnetic circuit, with the black arrows indicating the magnetization of the PP. Because the magnetic flux concentrates at the corner of a highly permeable material, a strong reverse field acts on the edges of PMs contacting the corners of the PPs (O'Shea *et al.*, 2010; Bizen *et al.*, 2018), indicated by circles. As a result, each PM may be locally demagnetized if H_{cj} is not sufficiently high compared with the reverse field. More probably, the magnetization can be reversed in the local area where the reverse field is higher than H_{cj}, resulting in a significant reduction in the undulator peak field. Although the local demagnetization can be avoided by

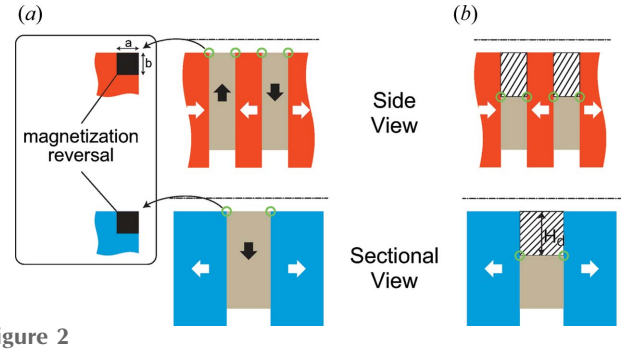

Figure 2
Magnetization of PMs and PPs at room temperature when (*a*) the whole PP is made of VP and (*b*) the inner PP (hatched area) is made of MXDy, being a non-magnetic material at room temperature. The circles indicate the positions where a strong reverse field is generated.

chamfering the PMs and PPs, the resultant peak field is lower than what is available under ideal conditions.

The above problem is more serious for short-period undulators, in which the volume of each PM is small, and thus we need to select a PM material with sufficiently high H_{cj}. Because B_r is negatively correlated with H_{cj}, the strong and localized reverse field effectively puts a limit on the attainable performance of conventional undulators using VP PPs.

Next, we consider the case where the inner PP is made of MXDy. Before being cooled down below the Curie temperature and turning into a ferromagnetic, it behaves as a non-magnetic material. Then the flux-concentrating points, which potentially cause the local magnetization reversal, are located below the inner surface of the PMs as shown in Fig. 2(*b*). It is obvious that their impact on the practical undulator performance is much lower than that of those in Fig. 2(*a*). Although the flux-concentrating points move to the inner surface when the MXDy PP is cooled down, H_{cj} is simultaneously enhanced by a large factor (of around 4 below 100 K), and thus the local magnetization reversal can be avoided. In summary, utilization of MXDy (or at least Dy) makes the selection of PM material more flexible.

3. Demonstration experiments

To demonstrate the performance of the MXDy PPs, we built a five-period prototype undulator with λ_u = 8 mm, using inner and outer PPs made of MXDy and VP, respectively, together with PMs made of PrFeB with B_r = 1.40 T and H_{cj} = 1.68 MA m^{-1} at room temperature (295 K), and B_r = 1.67 T and H_{cj} = 6.21 MA m^{-1} at 77 K. Note that half of the PPs were made of a single piece of VP to compare the performance between VP and MXDy. In the following sections, we describe the details of the prototype undulator and the experimental results. For reference, the specifications and parameters of the prototype undulator are summarized in Table 1.

3.1. Specifications of the prototype undulator

To determine the dimensions of the PMs and PPs, we performed numerical simulations with the computer code

Table 1
Specifications and parameters of the prototype undulator.

Parameter	Value
B_r	1.40 T (295 K), 1.67 T (77 K)
H_{cj}	1.68 MA m^{-1} (295 K), 6.21 MA m^{-1} (77 K)
λ_u	8 mm
L_m	2 mm
W_m	18 mm
H_m	17 mm
L_p	2 mm
W_p	2.3 mm
H_p	14 mm
H_d	4 mm

RADIA (Chubar *et al.*, 1998). As an example, peak fields at a gap of 2.5 mm computed as a function of W_p, H_d and L_p are plotted in Figs. 3(*a*), 3(*b*) and 3(*c*), respectively, with dashed lines indicating the actual dimensions chosen for the prototype undulator. It is obvious that W_p = 2.3 mm is optimized, while we need some explanation for the other two parameters.

The height of the MXDy PP (H_d = 4 mm) has been determined not only to enhance the peak field, but also to reduce the volume of MXDy pieces; in practice, a larger H_d does not significantly improve the expected performance. The pole length (L_p = 2 mm) and magnet length ($L_m = \lambda_u/2 - L_p$ = 2 mm) have been determined to facilitate assembling both the PPs and PMs.

The other dimensions, W_m = 18 mm, H_m = 17 mm and H_p = 14 mm, have been determined to be sufficiently large so that the resultant peak field is similar to what is expected when these dimensions are infinitely large.

Fig. 4(*a*) illustrates the three-dimensional structure of the prototype undulator. The PrFeB PMs were assembled in holders made of copper with clamps made of stainless steel, and the MXDy and VP PPs were glued to the PMs. The holders were then mounted on a pair of girders made of aluminium alloy to form the magnetic circuit shown in Fig. 1(*b*).

It should be mentioned that the use of any glue is generally unacceptable in an ultrahigh-vacuum and high-radiation environment; we thus need to use an alternative method in the actual device for reliable operation in the accelerator.

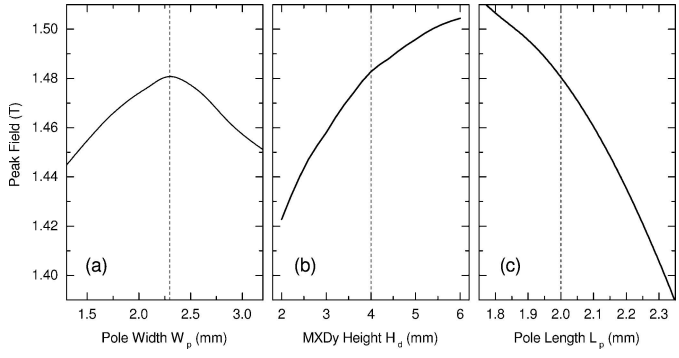

Figure 3
Examples of numerical simulations to determine the dimensions of PMs and PPs. The peak fields are plotted as a function of (*a*) W_p, (*b*) H_d and (*c*) L_p.

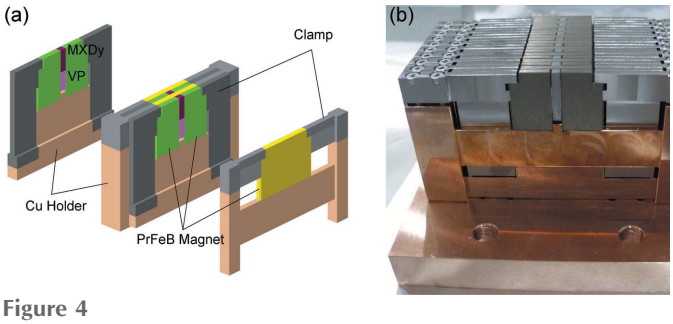

Figure 4
The structure of the prototype undulator for the demonstration experiments. (*a*) A three-dimensional view of the MXDy and VP PPs, PrFeB magnets, holders and clamps. (*b*) A picture of one of the two girders after assembly.

Fig. 4(*b*) shows an overall picture of one of the two girders after assembly. Note that the PP seen in the picture is made of a single piece of VP; the MXDy PPs are located on the opposite side.

After assembling all the elements, we measured the profile of the inner surface of each girder by means of an optical three-dimensional profiler to evaluate the gap value accurately; we found that the actual gap values at the VP and MXDy PPs were ∼0.15 mm and ∼0.1 mm narrower than the nominal value, respectively. These values are taken into account in the comparison between the numerical and experimental results to be discussed later.

3.2. Experimental results

After the surface profile measurement, the girders were rigidly fixed onto a supporting block, with a spacer to define the nominal gap inserted in between, whose thickness was changed discretely to adjust the nominal gap. The apparatus was then installed in a vacuum chamber with the supporting block being connected to a cryocooler head to cool down the whole structure. A Hall sensor, which was mounted on a vacuum-compatible three-axis linear stage, was also installed to measure the magnetic field distribution. The temperature of the prototype undulator was measured with a platinum resistance thermometer (PT100) attached to one of the copper holders to hold the PMs, with which we found that the lowest temperature reached 53 K, well below the Curie temperature of Dy.

Fig. 5 shows the magnetic field distribution at a nominal gap of 2.5 mm, measured by moving the Hall sensor along the z axis, where the dashed and solid lines show the measurement results before and after cooling, respectively. Note that the MXDy PPs were located on the downstream side. We clearly identify five peak positions corresponding to the VP PPs and four positions corresponding to the MXDy ones, where the peak field is enhanced by a factor of ∼2.4 after cooling down because of the ferromagnetic transition of MXDy. Note that the fifth peak position of the MXDy PP could not be measured because of the limited stroke of the linear stage. We then averaged the peak fields generated at the VP and MXDy PPs

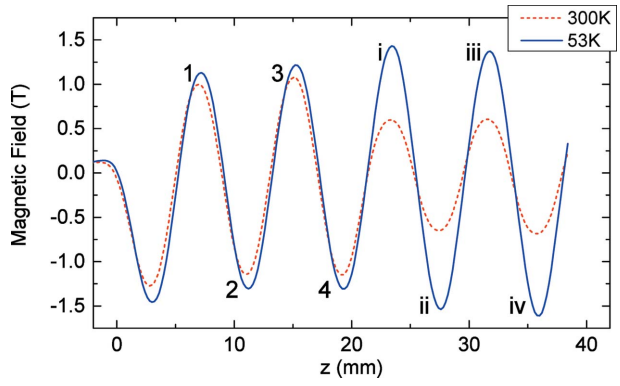

Figure 5
Magnetic field distributions along z, measured before and after cooling. Arabic and roman numbers indicate the averaged peak fields generated at the VP and MXDy PPs over the four peak positions, respectively.

over the four peak positions indicated in arabic and roman numbers, respectively.

We repeated the above process to measure the average peak field, B_p, generated by the VP and MXDy PPs for two other nominal gap values of 2.0 and 3.5 mm. The results are plotted as open squares (VP) and circles (MXDy) in Fig. 6 as a function of the actual gap value instead of the nominal one, which was evaluated using the measured surface profiles of the girders. To facilitate the following discussion, we performed curve fitting with a decaying exponential function, $B_p(g) = B_0 \exp(-ag)$, with B_0 and a being the fitting parameters. Note that a quadratic term in the exponent, which is in general necessary to represent the peak field of the undulator over a wide gap range, has been neglected, because we have just three data points within a narrow gap range. The resultant fitting curves are plotted as dashed (VP) and solid (MXDy) lines.

To examine the above experimental results, we computed the peak fields generated by the VP and MXDy PPs under the

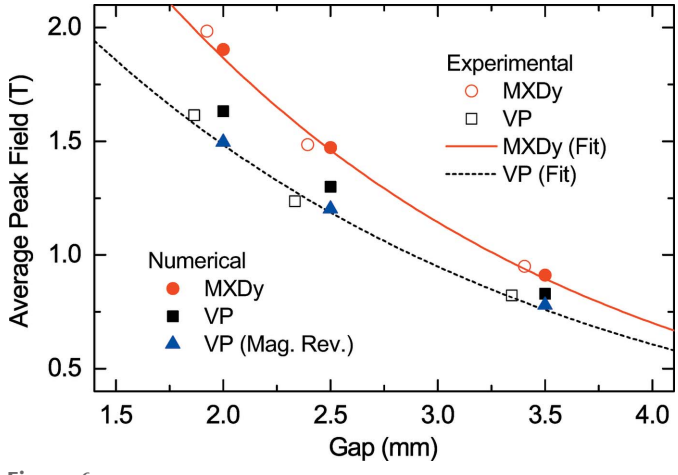

Figure 6
Measured and computed peak fields generated at the VP and MXDy PPs for the three different gap values. The solid and dotted lines indicate the fitting curves of the measured data. Triangles indicate the numerical values assuming magnetization reversal in the 0.3 mm × 0.3 mm area shown in Fig. 2(*a*).

experimental conditions. The results of the computation are plotted as filled rectangles (VP) and circles (MXDy) in Fig. 6, where we have assumed that the MXDy has magnetic properties of $\mu_i = 1000$ and $B_s = 3.5$ T. We find that the numerical results for the MXDy PPs agree well with the experimental ones, which is not the case for the VP PPs, where the numerical results are slightly higher than the experimental ones. This is probably attributable to the local magnetization reversal at the edges of the PMs exposed to a strong reverse field. In practice, $H_{cj} = 1.68$ MA m^{-1} at 295 K, or $\mu_0 H_{cj} = 2.11$ T with μ_0 being the vacuum permeability, is not sufficiently large to withstand fully the reverse field generated by the VP PP with $B_s = 2.35$ T, and thus the local area near the edge can encounter magnetization reversal before cooling down.

Based on the above considerations, we computed the peak field by the VP PP with an assumption that magnetization reversal occurs at the edges of PMs contacting the PPs, as shown in the inset of Fig. 2(*a*), in the area of $a \times b = 0.3$ mm $\times$ 0.3 mm in each PM. The results are plotted as solid triangles in Fig. 6 and are in good agreement with the fitting curve for the experimental results, suggesting the validity of the above assumption.

Now let us quantitatively discuss the advantage of the MXDy PP. From the fitting curves shown in Fig. 6, we find that the peak field is enhanced by 20, 23 and 27% at gaps of 3, 2.5 and 2 mm, respectively. Although we need to discuss the possibility of operating the undulator with such a narrow gap, these numbers are large enough to validate the utilization of MXDy PPs.

4. Drawbacks and countermeasures

Finally, we discuss the drawbacks of the proposed undulator based on narrow MXDy PPs, in terms of (i) the manufacturing cost of the MXDy PPs, and (ii) the impact of a narrow PP on the electron beam.

To discuss the first issue, we turn to the cost of MXDy PPs and PM blocks required to build the prototype undulator used in the experiment as an example. In spite of the large difference (an order of magnitude or larger) in the manufacturing cost per unit volume, the total cost of MXDy PPs is just three times higher than that of the PM blocks, thanks to the much smaller volume and fewer (one third) pieces. Although it is out of the scope of this paper to discuss whether this is acceptable, we note that the cost of PMs in typical undulators, in particular cryogenic ones, is just a fraction of the total cost of the whole undulator system composed of a huge number of components. In addition, the cost of MXDy is expected to be greatly reduced if we apply an adequate mass-production process.

The second issue is related to the so-called dynamic multipole (Safranek *et al.*, 2002; Bahrdt & Wüstefeld, 2011), which comes from a relatively large dependence of the peak field on the horizontal position (x). As an example, let us consider an ideal undulator without any errors, which has the same parameters as the prototype undulator used in the experiments except that the number of periods is 100. We

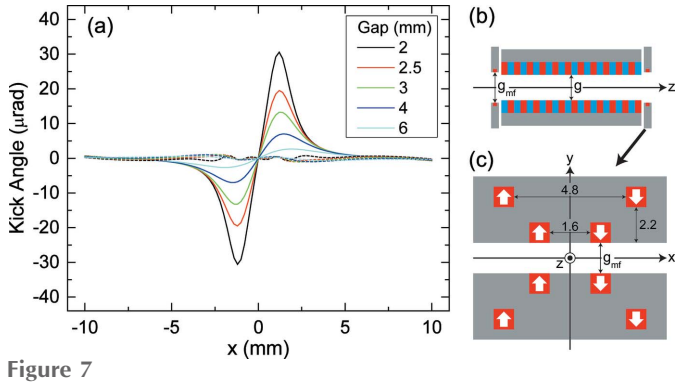

Figure 7
The dynamic multipole and its correction. (*a*) Position-dependent kick angles computed for 6 GeV electrons passing through a 100 period undulator having the same parameters as those in the experiment. (*b*) A drawing of the independent magic fingers. (*c*) An example of the PM arrangement (dimensions in millimetres).

computed kick angles for 6 GeV electrons passing though this undulator with different horizontal positions, which are plotted as solid lines in Fig. 7(*a*) for different gap values. Even with ideal PMs and PPs, a horizontally displaced electron is kicked with an angle depending on x. In other words, the undulator has a multipole field component, which can potentially lower the injection efficiency and shorten the beam lifetime in storage rings.

It is well known that the dynamic multipole mentioned above can be corrected by the so-called current-strip scheme (Bahrdt *et al.*, 2008), in which a number of wires located between the electron beam and PMs work to correct the different kick angles. It is obvious, however, that this scheme may be difficult to apply to short-period undulators, in which the PMs and PPs are located inside the vacuum chamber with a narrow gap between the top and bottom girders.

To overcome the above problem, let us consider multipole trim magnets, *i.e.* another correction scheme also referred to as the 'magic finger' (Hoyer *et al.*, 1995), in which a number of tiny PMs are placed at both ends of an undulator and arranged to correct the position-dependent kicks. In general, holders accommodating these tiny PMs are attached directly to the ends of the magnetic girders and cannot be operated separately; in other words, the gap between the top and bottom holders is identical to that of the undulator. As a result, the arrangement of PMs at a specific gap value is not necessarily effective at other gap values. We thus propose to separate the mechanical system for the magic finger from that for the undulator, as illustrated in Fig. 7(*b*), so that the gap of the magic finger (g_{mf}) can be chosen independently of that of the undulator (g).

As an example, we show the results of this correction as dashed lines in Fig. 7(*a*), using magic fingers composed of eight identical PMs arranged as illustrated in Fig. 7(*c*), whose gap is adjusted according to a simple relation $g_{mf} = 1.5g - 1$ ($g \geq 2$ mm). Note that the width, height and length of each PM are 0.8, 1.0 and 1.5 mm, respectively. Although these parameters are roughly optimized based on a heuristic approach, we find that the kick angles are reduced down to at most 1 μrad. The residual kick errors can be further reduced if

necessary with a more dedicated optimization scheme, and/or additional magic fingers.

5. Conclusions

We have experimentally demonstrated the enhancement of undulator performance using MXDy PPs. We now discuss their importance in the development of subcentimetre-period CPMUs in comparison with superconducting undulators (SCUs), *i.e.* another approach to enhance the performance of short-period undulators.

As reported in a previous theoretical report (Bahrdt & Ivanyushenkov, 2013), the subcentimetre period corresponds to the so-called crossover period, where the performances of (conventional) CPMUs and SCUs are comparable. To be more specific, SCUs can generate a much stronger field only if the period is considerably longer than 10 mm. In practice, existing SCUs running in synchrotron radiation facilities have a period of around 15 mm (Casalbuoni *et al.*, 2006, 2016; Ivanyushenkov *et al.*, 2015). This in turn gives a good reason to develop subcentimetre-period CPMUs, although the achievable peak field is not sufficiently strong for many applications. It is obvious that the MXDy PPs demonstrated experimentally in this work, together with the proposed multipole correction scheme, will greatly contribute to enhancing the performance of such undulators.

References

Bahrdt, J. (2011). *Proceedings of the 33rd International Free Electron Laser Conference (FEL2011)*, 22–26 August 2011, Shanghai, China, pp. 435–442. THOAI1.

Bahrdt, J., Frentrup, W., Gaupp, A., Scheer, M. & Wuestefeld, G. (2008). *Proceedings of the 11th European Particle Accelerator Conference (EPAC08)*, 23–27 June 2008, Genoa, Italy, pp. 2222–2224. WEPC097.

Bahrdt, J. & Ivanyushenkov, Y. (2013). *J. Phys. Conf. Ser.* **425**, 032001.

Bahrdt, J. & Kuhn, C. (2015). *Synchrotron Radiat. News*, **28**(3), 9–14.

Bahrdt, J. & Wüstefeld, G. (2011). *Phys. Rev. ST Accel. Beams*, **14**, 040703.

Behrendt, D. R., Legvold, S. & Spedding, F. H. (1958). *Phys. Rev.* **109**, 1544–1547.

Benabderrahmane, C., Valléau, M., Ghaith, A., Berteaud, P., Chapuis, L., Marteau, F., Briquez, F., Marcouillé, O., Marlats, J.-L., Tavakoli, K., Mary, A., Zerbib, D., Lestrade, A., Louvet, M., Brunelle, P., Medjoubi, K., Herbeaux, C., Béchu, N., Rommeluere, P., Somogyi, A., Chubar, O., Kitegi, C. & Couprie, M.-E. (2017). *Phys. Rev. Accel. Beams*, **20**, 033201.

Bizen, T., Kinjo, R. & Tanaka, T. (2018). *Phys. Rev. Lett.* **121**, 124801.

Calvi, M., Schmidt, T., Anghel, A., Cervellino, A., Leake, S. J., Willmott, P. R. & Tanaka, T. (2013). *J. Phys. Conf. Ser.* **425**, 032017.

Casalbuoni, S., Cecilia, A., Gerstl, S., Glamann, N., Grau, A., Holubek, T., Meuter, C., de Jauregui, D. S., Voutta, R., Boffo, C., Gerhard, T., Turenne, M. & Walter, W. (2016). *AIP Conf. Proc.* **1741**, 020002.

Casalbuoni, S., Hagelstein, M., Kostka, B., Rossmanith, R., Weisser, M., Steffens, E., Bernhard, A., Wollmann, D. & Baumbach, T. (2006). *Phys. Rev. ST Accel. Beams*, **9**, 010702.

Chang, C. H., Hwang, C. S., Huang, M., Lin, F. Y., Chen, H. H., Fan, T. C. & Hsu, K. T. (1998). *Proceedings of the Sixth European Particle Accelerator Conference (EPAC98)*, 22–26 June 1998, Stockholm, Sweden, pp. 2210–2212.

Chavanne, J., Penel, C. & Elleaume, P. (2009). *Synchrotron Radiat. News*, **22**(4), 34–37.

Chavanne, J., Van Vaerenbergh, P. & Elleaume, P. (1999). *Nucl. Instrum. Methods Phys. Res. A*, **421**, 352–360.

Chubar, O., Elleaume, P. & Chavanne, J. (1998). *J. Synchrotron Rad.* **5**, 481–484.

García, L. M., Chaboy, J., Bartolomé, F. & Goedkoop, J. B. (2000). *Phys. Rev. Lett.* **85**, 429–432.

Hara, T., Tanaka, T., Kitamura, H., Bizen, T., Maréchal, X., Seike, T., Kohda, T. & Matsuura, Y. (2004). *Phys. Rev. ST Accel. Beams*, **7**, 050702.

Hoyer, E., Marks, S., Pipersky, P. & Schlueter, R. (1995). *Rev. Sci. Instrum.* **66**, 1901–1903.

Ivanyushenkov, Y., Harkay, K., Abliz, M., Boon, L., Borland, M., Capatina, D., Collins, J., Decker, G., Dejus, R., Dooling, J., Doose, C., Emery, L., Fuerst, J., Gagliano, J., Hasse, Q., Jaski, M., Kasa, M., Kim, S. H., Kustom, R., Lang, J. C., Liu, J., Moog, E., Robinson, D., Sajaev, V., Schroeder, K., Sereno, N., Shiroyanagi, Y., Skiadopoulos, D., Smith, M., Sun, X., Trakhtenberg, E., Vasserman, I., Vella, A., Xiao, A., Xu, J., Zholents, A., Gluskin, E., Lev, V., Mezentsev, N., Syrovatin, V., Tsukanov, V., Makarov, A., Pfotenhauer, J. & Potratz, D. (2015). *Phys. Rev. ST Accel. Beams*, **18**, 040703.

Murokh, A., Solovyov, V., Agustsson, R., O'Shea, F. H., Chubar, O., Chen, Y. & Grandsaert, T. (2014). *Nucl. Instrum. Methods Phys. Res. A*, **735**, 521–527.

Nakamura, N., Koseki, T., Fujisawa, M., Kamiya, Y., Kobayashi, H., Ohashi, K., Tsukino, N., Kawai, T. & Kawai, M. (1998). *Proceedings of the First Asian Particle Accelerator Conference (APAC98)*, 23–27 March 1998, Tsukuba, Japan, pp. 689–691. 6d010.

O'Shea, F. H., Agustsson, R., Chen, Y.-C., Grandsaert, T., Murokh, A., Woods, K., Solovyav, V., Park, J.-H. & Stillwell, R. (2013). *Proceedings of the Fourth International Particle Accelerator Conference (IPAC2013)*, 12–17 May 2013, Shanghai, China, pp. 2298–2300. WEPWA081.

O'Shea, F. H., Marcus, G., Rosenzweig, J. B., Scheer, M., Bahrdt, J., Weingartner, R., Gaupp, A. & Grüner, F. (2010). *Phys. Rev. ST Accel. Beams*, **13**, 070702.

Ostenfeld, C. & Pedersen, M. (2010). *Proceedings of the First International Particle Accelerator Conference (IPAC2010)*, 23–28 May 2010, Kyoto, Japan, pp. 3093–3095. WEPD006.

Safranek, J., Limborg, C., Terebilo, A., Blomqvist, K. I., Elleaume, P. & Nosochkov, Y. (2002). *Phys. Rev. ST Accel. Beams*, **5**, 010701.

Swift, W. & Mathur, M. (1974). *IEEE Trans. Magn.* **10**, 308–313.